Pattern Recognition 47 (2014) 721–735

Contents lists available at ScienceDirect

Pattern Recognition

journal homepage: www.elsevier.com/locate/pr

Probabilistic pseudo-morphology for grayscale and color images ☆

Alexandru Căliman [a,*], Mihai Ivanovici [a], Noël Richard [b]

[a] MIV² Laboratory, Department of Electronics and Computers, Transilvania University, Braşov 500024, România
[b] XLIM-SIC UMR CNRS 6172, Signals, Images and Communications Laboratory, University of Poitiers, France

ARTICLE INFO

Article history:
Received 1 March 2013
Received in revised form
17 July 2013
Accepted 23 August 2013
Available online 4 September 2013

Keywords:
Mathematical morphology
Fractal dimension
Texture analysis

ABSTRACT

Mathematical morphology offers popular image processing tools, successfully used for binary and grayscale images. Recently, its extension to color images has become of interest and several approaches were proposed. Due to various issues arising from the vectorial nature of the data, none of them imposed as a generally valid solution. We propose a probabilistic pseudo-morphological approach, by estimating two pseudo-extrema based on Chebyshev inequality. The framework embeds a parameter which allows controlling the linear versus non-linear behavior of the probabilistic pseudo-morphological operators. We compare our approach for grayscale images with the classical morphology and we emphasize the impact of this parameter on the results. Then, we extend the approach to color images, using principal component analysis. As validation criteria, we use the estimation of the color fractal dimension, color textured image segmentation and color texture classification. Furthermore, we compare our proposed method against two widely used approaches, one morphological and one pseudo-morphological.

1. Introduction

The mathematical morphology (MM) was founded by Matheron [1] and Serra [2] and became very popular in non-linear image processing. Initially, the MM had been introduced as a processing technique for binary images, which were regarded as sets; therefore, its elementary operations are based on the set theory [3]. However, the extension to sets of grayscale images, using the *umbra* concept [4,5], introduced a generalization of the basic morphological operations which were subsequently used in many image processing and analysis methods e.g. morphological filtering [6], watershed segmentation [7], etc. The grayscale morphology is based on the lattice theory, which implies a partial ordering of the data within the grayscale images. In this case, the lattice structure is not difficult to obtain, since the grayscale images are real functions and the set of real numbers implicitly possesses a lattice structure. However, while the extension from binary to grayscale images is a natural one, the extension to color or multi-spectral images is not straightforward, because of the vectorial nature of the data and the difficulty in finding a suitable ordering for it. Barnett introduced four types of vector orderings: marginal, reduced, conditional and partial [8]. When applied to color data, all these orderings have certain disadvantages, depending on application. For instance, the marginal ordering introduces false colors and the conditional ordering generates visual non-linearities from the human perception point of view [9]; the reduced and partial orderings are either relying on pre-orderings, thus lacking the anti-symmetry property, or behave like conditional orderings, generating perceptual non-linearities. In fact, the difficulty of extending MM to multivariate data does not consist in obtaining an ordering, but in obtaining a pertinent ordering from the human visual system point of view. There have been proposed a plethora of methods for color and multivariate MM, but few of them, only recently, referred to this linearity problem [10,11]. The paper written by Aptoula and Lefèvre in 2007 [12], which includes more than 70 references to different color MM methods, represents a relatively recent and comprehensive state-of-the-art in this field. Nevertheless, other approaches have been introduced recently. For instance, in [13] a method using the color data distribution in a partial ordering based on depth functions is presented, [14] proposes a graph-based approach using the Laplacian eigenmaps as a method for non-linear dimensionality reduction, thus resulting a reduced ordering, while[15] proposes a geometrical method based on the so-called Loewner order. Recently, there has also been a great interest in supervised methods for establishing orderings among vectorial data [16,17].

In addition to the proposed morphological approaches whose operations respect all the mathematical properties of the classical MM, there were also proposed pseudo-morphologies, which do not require an underlying order among the image data, focusing on computing directly the minimum and maximum of a given set [18,19]. This kind of approaches do not require a complete lattice

☆This paper is partially supported by the Sectoral Operational Programme Human Resources Development (SOP HRD), ID76945 financed from the European Social Fund and by the Romanian Government.

* Corresponding author. Tel.: +40 268475751.
E-mail addresses: alexandru.caliman@gmail.com (A. Căliman), mihai.ivanovici@unitbv.ro (M. Ivanovici), noel.richard@univ-poitiers.fr (N. Richard).

0031-3203/$ - see front matter © 2013 Elsevier Ltd. All rights reserved.
http://dx.doi.org/10.1016/j.patcog.2013.08.021

structure, consequently lacking a binary relation that is reflexive, anti-symmetric and transitive and thus, they cannot be theoretically considered *morphological*. However, they could be of practical interest in noise reduction, texture classification or multispectral remote sensing data processing [20,21].

In this paper we propose a probabilistic pseudo-morphology (PPM) approach based on the Chebyshev inequality, in which we estimate the two extrema (the *infimum* and the *supremum*) of a set instead of defining an underlying ordering for the entire data set. PPM is based on the choice of one parameter, which is capable of turning it either into a linear or non-linear approach (see details in Section 3). By using the statistical moments (both the mean and the variance) of the local data distribution, the proposed method is less influenced by the presence of noise. Then, we propose an extension to color or multivariate images. This extension has the advantages that it is full-vectorial and it generates adjustable operations i.e. linear versus non-linear vector filtering. Despite the fact that it introduces *false colors*, it is useful in various applications like morphological edge detection or texture description based on morphological operations. We demonstrate the usefulness of our approach in the context of color texture complexity estimation, textured image segmentation and color texture classification.

The next sections of the paper are organized as follows: Section 2 presents the general concepts and definitions for MM and Chebyshev inequality, on which our approach is based; Section 3 defines the probabilistic pseudo-morphology for grayscale images while in Section 4 the extension to multivariate images is presented; the paper is ended with a section of discussions and one of conclusions.

2. Theoretical notions

2.1. General aspects about MM

In this section we briefly present the general concepts and definitions of MM's basic operations, using the notations from [22]. Table 1 presents all the notations we use and propose within this article.

The erosion and the dilation, the fundamental operations of MM, are defined within a complete lattice as the operations which distribute over the infima and the suprema [3]. However, these definitions are not suitable for a practical implementation. The more popular definitions, which are often used in implementations, are based on the concept of *structuring element* (SE), which is a relatively small set used for probing the image f, which is analyzed. An origin is associated with any SE g, within its definition domain $\mathcal{D}_g$. This origin helps positioning the SE at every coordinate within the initial image definition domain $\mathcal{D}_f$ i.e. at every pixel coordinate x. In order to avoid mixing the spatial units of $\mathcal{D}_f$ with the pixel values $C_x \in \mathcal{S}_{\mathcal{D}f}$ ($\mathcal{S}_{\mathcal{D}f} \subset \mathbb{R}$ for grayscale images or $\mathcal{S}_{\mathcal{D}f} \subset \mathbb{R}^n$ for multivariate images) and because of the fact that there is no pertinent meaning of adding two multivariate image data, it is very common to use *flat* SEs, which are defined only through their origin and their shape, given by $\mathcal{D}_g$. Using these notations, the erosion and the dilation of an image f, using a *flat* SE g, are defined as follows [23]:

$$[\varepsilon_g(f)](x) = \bigwedge_{z \in \mathcal{D}_g} f(x+z), \quad \forall x \in \mathcal{D}_f \tag{1}$$

$$[\delta_g(f)](x) = \bigvee_{z \in \mathcal{D}_g} f(x-z), \quad \forall x \in \mathcal{D}_f \tag{2}$$

where $\bigwedge$ and $\bigvee$ are the *infimum* and *supremum* operators. It can be noticed that the basic morphological operations involve finding an infimum and a supremum for the points within a local region, given by the SE positioning. The extension of these operations to multivariate images is not straightforward, due to the difficulty of defining such extrema for vectorial data.

Table 1
Notations.

f, $\mathcal{D}_f$	Image function and its support
$\mathcal{S}_{\mathcal{D}f}$	The f function's range of values
$\widetilde{\mathcal{S}_{\mathcal{D}f}}$	The f function's codomain expressed in PCA basis
$x=(i,j)$	Spatial coordinates for the pixel at line i and column j
C_x, $\widetilde{C_x}$	Grayscale, color or multivariate coordinates of the x pixel, expressed in the initial or PCA space
g, $\mathcal{D}_g$	Structuring element and its spatial domain of definition
$[\delta_g(f)](x)$, $[\varepsilon_g(f)](x)$	Dilation and erosion of image f, using the structuring element g, computed for pixel x
ξ, μ_ξ, σ_ξ	A random variable, its mean value and standard deviation
$\mathfrak{E}_\alpha$, $\mathfrak{E}_\beta$	Probabilistic pseudo-extrema
$(\Re_i^+, \Re_i^-)$	The ith pair of global references

2.2. The Chebyshev inequality

Our approach is based on the Chebyshev inequality (3), which expresses the upper bound of the probability that any random variable ξ takes values farther from its average value, outside of a specified interval [24]. The inequality stands for any distribution, as long as the mean and the standard deviation are finite [25]. Let ξ be a random variable with the mean μ_ξ and the standard deviation σ_ξ; the Chebyshev inequality states that

$$P\{|\xi-\mu_\xi| \geq k\sigma_\xi\} \leq \frac{1}{k^2}. \tag{3}$$

Using the k parameter, one may generate symmetrical intervals around the mean value, delimited by bounds which are more or less closed to the real maximum or minimum values of the distribution. The bounds of this confidence interval are given by (4). We define these bounds as the probabilistic pseudo-extrema, $\mathcal{E}^+$ and $\mathcal{E}^-$, in the sense of the Chebyshev inequality:

$$\begin{cases} \mathcal{E}^+ & \triangleq \mu_\xi + k\sigma_\xi \\ \mathcal{E}^- & \triangleq \mu_\xi - k\sigma_\xi \end{cases} \tag{4}$$

Using an appropriate k value, the probabilistic extrema and the real maximum and minimum values may be more or less closed to each other, but only for symmetrical distributions there is a unique k for which they coincide.

3. A direct application for grayscale images

Our first proposal aims at the direct application of the previously described notions to grayscale images. Thus, we consider an image $f : \mathcal{D}_f \to \mathcal{S}_{\mathcal{D}f}$, with $\mathcal{S}_{\mathcal{D}f} \subset \mathbb{R}$. The histogram of any local neighborhood of the image is an estimate of the probability density function associated with the pixel data. In this case, the Chebyshev inequality defines an interval depending on the k parameter and the standard deviation of the pixel values. The error between the real maximum and minimum of the local data set and the estimated pseudo-extrema based on the Chebyshev's inequality is a function of k. We define the grayscale pseudo-dilation and pseudo-erosion operations as

$$[\varepsilon_g(f)](x) = \bigwedge_{z \in \mathcal{D}_g} f(x+z) \triangleq \mu_\xi - k\sigma_\xi, \quad \forall x \in \mathcal{D}_f \tag{5}$$

$$[\delta_g(f)](x) = \bigvee_{z \in \mathcal{D}_g} f(x-z) \triangleq \mu_\xi + k\sigma_\xi, \quad \forall x \in \mathcal{D}_f \tag{6}$$

where ξ represents the particular outcome of a random variable, modeling the intensity of the grayscale pixels given by $\mathcal{D}_f \cap \mathcal{D}_g$. Thus, μ_ξ and σ_ξ are computed locally, in a neighborhood given by the SE.

Fig. 1 shows the histogram of the grayscale "Lena" image of size 256×256. One may notice that for a k value close to 2, the error between the pseudo-extrema estimated by the Chebyshev inequality and the real maximum and minimum, computed for the entire image, is reduced. In fact, according to the Chebyshev inequality, for $k=2$, there is a probability smaller than 0.25 for any value to be outside the computed interval. In our particular case, it may be observed that the values which are outside of this interval are few, indicating that Chebyshev's relation gives an acceptable upper limit for this probability. Thus, in a first approximation, using values for k close to 2, the behavior of PPM should be similar with the behavior of the classical Gray-Level Mathematical Morphology (GLMM). However, this may not be always true, because within the local processings, this similarity between the estimated extrema and the real ones is influenced by the local data distribution which in many cases is different than the global distribution. For instance, a large skewness of the local distribution leads to the situation in which one of the pseudo-extremum is inside the data distribution hull, while the other is outside. Thus, estimations of the k value could be done for every local data set, according to certain additional information about its distribution. However, for practical purposes, within this work we chose the same k value for all the local pseudo-morphological processings. Thus, in what follows, we present results for three cases: (i) $k=0.2$, which generates pseudo-extrema close to the mean value, (ii) $k=2$, which leads to acceptable estimated extrema in the global case and (iii) $k=4$, a value which overpasses the optimal value for the global distribution. In order to obtain reasonably visible results for this paper, we chose SE sizes of 5×5 and 11×11. The original size images are available online at http://miv.unitbv.ro/ppm. What follows is a qualitative analysis of our results.

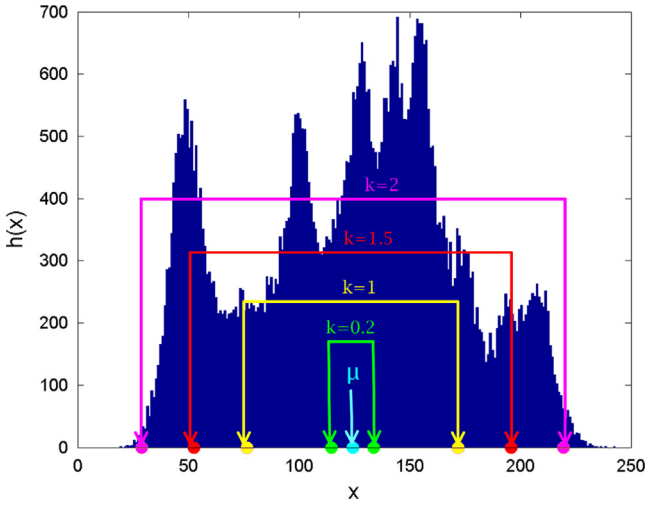

Fig. 1. Example of Chebyshev interval for the "Lena" image histogram for various values of k (0.2, 1, 1.5, 2).

Case (i), $k = 0.2$: As the estimated probabilistic pseudo-extrema for small k values are close to the mean value of the local data defined by the SE, the PPM behavior tends to be close to a smoothing filter (see the results for $k=0.2$ in Fig. 4). In this case, the PPM operations exhibit a behavior which is more similar to a linear filter rather than to non-linear classical morphological filters obtained through min/max operators.

Case (ii): When $k=2$, which is a value defining a bound close to the real global extrema, the behavior is close to the classical GLMM (see the first and the third column of Figs. 2 and 3). At this point, it is interesting to note that some parallels could be made between the rank filters and PPM for certain values of k. However, the PPM could not be assimilated to a rank filter because we did not order all the pixel values inside the data set, we just defined the pseudo-extrema through a statistical model given by the Chebyshev inequality. Nevertheless, according to particular k values, the process generates results which are close to certain particular rankings inside a completely ordered data set.

Analyzing the results one may notice some interesting facts: first, comparing the erosion and pseudo-erosion obtained using a SE of size 11×11, it may be noticed that the classical approach introduces some artifacts due to the particular local distributions (e.g. at the top of the hat). Thanks to the statistical filtering intrinsic to PPM, by opposition to the classical approach, the shape of the SE is not visible in the results and the pseudo-eroded image does not present this kind of artifacts. The second element of interest lies in the ability to preserve the morphological details. For instance, in the second and the third columns in Figs. 2 and 3, we observe that Lena's right eyebrow and nose shapes are better preserved than those obtained using the classical approach. The last element of interest could be observed in the hat feathers, within both Figs. 2 and 3, where the classical approach is perturbed by the complexity of the texture and the feathers

Fig. 2. Pseudo-erosion (PPM) for $k=2$ and the GLMM erosion using a *flat* SE, applied to "Lena" image for SE sizes 5×5 (top row) and 11×11 (bottom row).

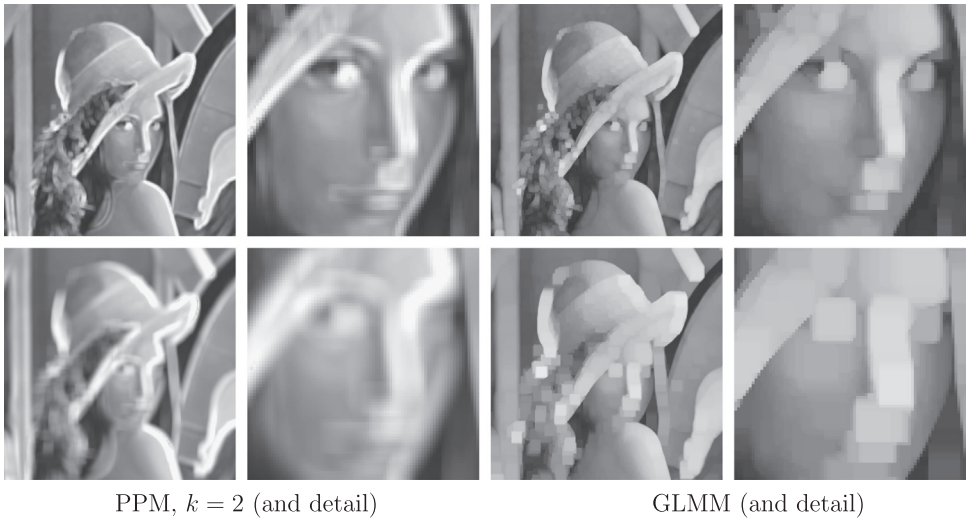

Fig. 3. Pseudo-dilation (PPM) for $k=2$ and the GLMM erosion using a *flat* SE, applied to "Lena" image for SE sizes 5×5 (top row) and 11×11 (bottom row).

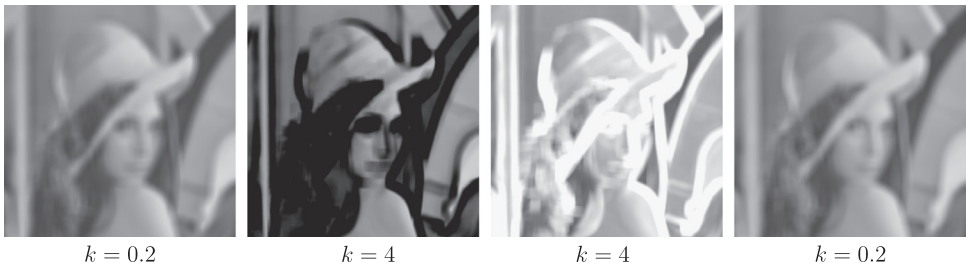

Fig. 4. Extreme cases of k for pseudo-erosions (left half) and pseudo-dilations (right half); 11×11 SE.

structure is quickly lost, depending on the SE size, while PPM keeps the respective textural structure. These remarks illustrate that the PPM approach is less sensitive to local noise, while better preserving the local structure than the classical approach.

Case (iii), $k = 4$: The case when k overpasses the optimal value for the global data is depicted in Fig. 4. In this last case, when k becomes very large, the probability that grayscale data exists outside the interval generated by the estimated extrema tends to be null, since the pseudo-extrema skyrockets to $-\infty$ and $+\infty$. However, considering that these pseudo-extrema represent grayscale pixel values and thus, they need to be within a given bounded interval, the resulted pixel values would be saturated (black and white). In this case, the behavior of the PPM is similar to the classical MM with a *non-flat* SE.

In addition to the qualitative analysis presented above, we also performed a quantitative evaluation of the performance of our approach, by computing the quadratic error between the images obtained using the classical GLMM with a *flat* SE and the PPM. The operations are performed on the grayscale "Lena" image and the error is measured for various values of the k parameter (see Fig. 5). At a first glance, one may notice that the error is minimum for a k value close to 2, which is the value chosen in Case (ii), presented above. It is interesting to observe that the optimal value is approximately the same for pseudo-dilation and pseudo-erosion, being related to the optimal k value for the global distribution (Fig. 1). However, this is just a particular case, since for the PPM approach the pseudo-extrema are estimated using local distributions which may differ significantly from the global one. The value of the quadratic error indicates that there is an optimum value of k for which our approach generates results which are close to the classical GLMM results. The minimum error normed by the image size corresponds to approximately 5% per pixel (on average), which could be reduced even further in an adaptive approach if

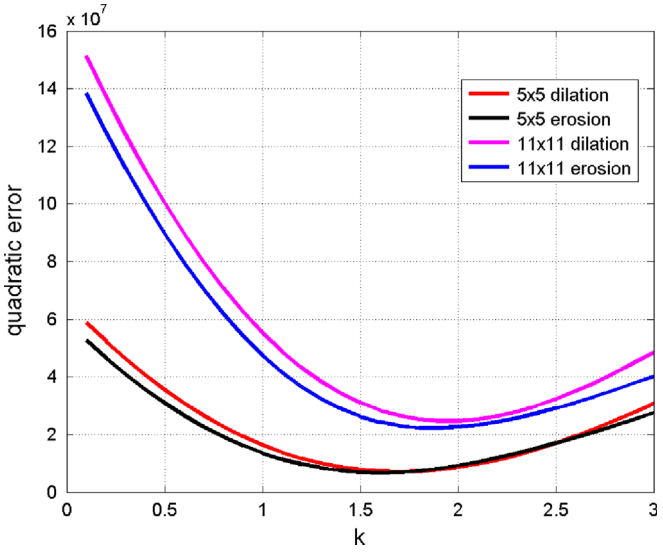

Fig. 5. Quadratic error between PPM and GLMM results as a function of k.

for each local distribution or even for each local pseudo-extremum estimation, different values would be appropriately chosen for k.

As a second validation criterion, we embraced the idea of using the estimation of the fractal dimension (FD) for grayscale images. Originally, Serra proposed the usage of the morphological operations for FD estimation [2], which was consequently described as the *covering blanket* approach by Peleg et al. [26] and Maragos and Sun [27]. More recently, Ledoux et al. [28] uses this measure as a validation criterion for color ordering approaches. The purpose of the *covering blanket* algorithm is to compute the volume comprised between an upper and a lower cover of the analyzed image,

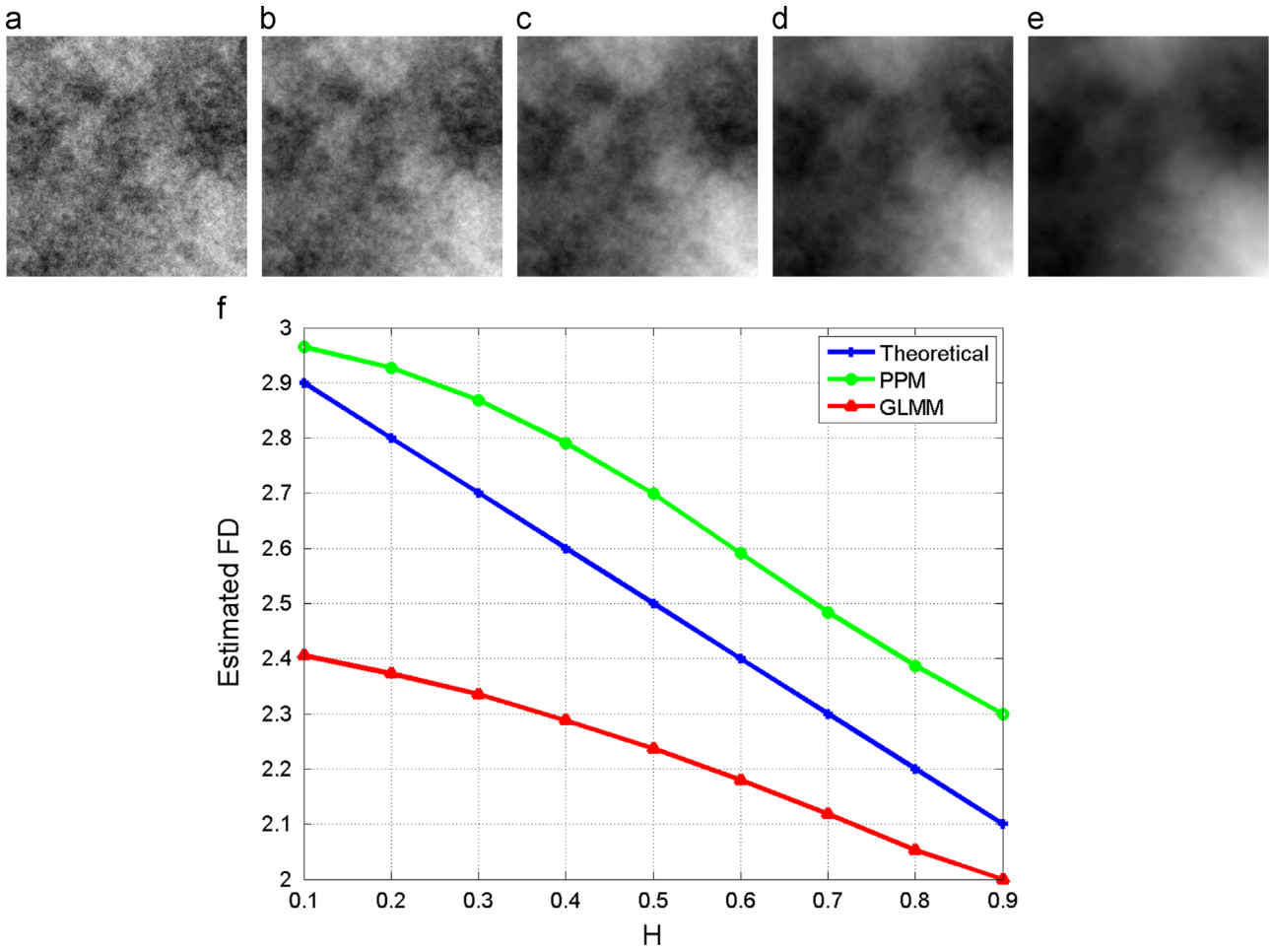

Fig. 6. Comparison between two estimated FDs, obtained using GLMM and PPM and the theoretical FD, for synthetic textures of varying complexity (top row). (a) $H=0.1$, (b) $H=0.3$, (c) $H=0.5$, (d) $H=0.7$, (e) $H=0.9$, and (f) comparison. (For interpretation of the references to color in this figure caption, the reader is referred to the web version of this article.)

obtained through the dilation and erosion of the initial image. The evolution of the volume as a function of the SE size is linked to the texture complexity, thus defining a multiscale feature used in numerous applications [27,29]. Consequently, in Fig. 6, we present a comparison between the theoretical and estimated FDs for synthetic textures of various complexities. The textures were generated using the *random midpoint displacement* method [30] for generating fractional Brownian motion, with a complexity given by the Hurst parameter H [31]. This real-valued parameter, comprised within $[0,1]$, is tightly related to the FD through the following relation, valid for grayscale fractal images:

$$FD = 3 - H \tag{7}$$

Thus, for small values of H, the complexity of the texture is high, the corresponding theoretical FD being close to 3. For H close to 1, the texture becomes less complex, close to a smooth surface, which has the theoretical FD=2. The results show that the PPM approach (green curve) leads to results which are more similar to the theoretical measure (blue curve) than the ones generated through GLMM. Moreover, the mean squared error (MSE) of the FD estimated using PPM is smaller (0.03) than the MSE of the FD estimated using GLMM (0.09). Consequently, the PPM approach offers a better estimation of texture complexity, not only in terms of ability of correct texture complexity ranking but also regarding the dynamic range.

As we previously presented, one of the advantages of PPM is that it integrates a statistical filtering, which makes it less sensitive to local noise and artifacts which are not necessarily related to the texture or shape complexity. By keeping more precisely the local textural structure during the iterative process, the texture evaluation is more precise. So, due to this possibility, our approach is more accurate in extracting texture features than the classical approach. In addition, the classical MM is rarely applied directly on original images; low-pass filters are often applied, to solve the kind of problems which we previously described. But such solutions raise the question of choosing among filters and requires an analysis of the impact of the cut-off band selection for the filter. With the PPM, we embed the answer to this question in an unique formalism, driven only by one parameter, k. Moreover, for the processing of color or multivariate images, simple low-pass filters for vectorial data do not exist and one of the major interests of our approach is the intrinsic answer to this question, provided by the approach itself.

4. Extension to color and multivariate images

For multivariate images, with pixel values C_x expressed in $\mathcal{S}_{\mathcal{D}f} \subset \mathbb{R}^3$ for color images and $\mathcal{S}_{\mathcal{D}f} \subset \mathbb{R}^n$ for the generic multivariate case, the purpose is to extract an n-dimensional interval in the sense of the Chebyshev inequality. Given the n-dimensional

vectors $C_x = (C_{x_0}, C_{x_1}, \ldots, C_{x_{(n-1)}})$, in a marginal approach, the direct extension is the following:

$$\bigwedge_{\substack{z \in \mathcal{D}_g \\ x \in \mathcal{D}_f}} f(x+z) = (\mathcal{E}^-_0, \ldots, \mathcal{E}^-_{(n-1)}) = (\mu_{\xi_0} - k\sigma_{\xi_0}, \ldots, \mu_{\xi_{(n-1)}} - k\sigma_{\xi_{(n-1)}}) \tag{8}$$

$$\bigvee_{\substack{z \in \mathcal{D}_g \\ x \in \mathcal{D}_f}} f(x-z) = (\mathcal{E}^+_0, \ldots, \mathcal{E}^+_{(n-1)}) = (\mu_{\xi_0} + k\sigma_{\xi_0}, \ldots, \mu_{\xi_{(n-1)}} + k\sigma_{\xi_{(n-1)}}) \tag{9}$$

in which μ_{ξ_i} and σ_{ξ_i} are computed from the local distributions given by $\mathcal{D}_f \cap \mathcal{D}_g$, for the ith component of C_x.

As defined by this construction, the multivariate extension introduces false colors: first, through the Chebyshev bound which does not extract an existing value from the initial distribution and second, by the marginal construction that separately extracts bounds for each channel before combining them into a vectorial bound. In order to limit the effect of the second factor and to objectively assess the variance of the data, the Principal Component Analysis (PCA) is applied, thus ensuring the validity of the estimated pseudo-extrema.

4.1. The PCA step

PCA allows defining a linear transformation that maximizes the variance of the multivariate data on certain directions. In our probabilistic extrema estimation context, PCA enhances the pseudo-extrema quality definition in the sense of the color data set. Given the existing correlation between the color channels for various color spaces, like RGB, PCA will correctly assess the variation of the multi-dimensional signal on the first principal component. Due to PCA, the data is expressed in a new coordinate system (denoted with "$\sim$" within this work – see Table 1), in which the first component is associated with the direction on which the variance of the signal is maximum. Thus, the new data channels may be prioritized: the highest priority is associated with $\widetilde{C_0}$, while $\widetilde{C_{(n-1)}}$ receives the lowest priority, since

$$\sigma^2_{\widetilde{\xi_0}} > \sigma^2_{\widetilde{\xi_1}} > \cdots > \sigma^2_{\widetilde{\xi_{(n-1)}}} \tag{10}$$

in which $\widetilde{\xi_i}$ represents the particular outcome of a random variable, modeling the ith component of the data, after PCA. In addition, the PCA axis is orthogonal with each other and the data components are uncorrelated, thus the distribution would be more suitable for a marginal definition of the extrema. However, we are mainly interested in a full-vectorial approach, rather than the marginal definition given by (8) and (9).

4.2. Drawbacks of the PCA

The PCA approach only determines the directions on which the data variance is maximized and the data components are uncorrelated. However, in order to define an order between two points on a particular direction, a sense has to be associated with that direction. Nevertheless, we cannot automatically associate a sense to each of the generated axis because the directions are obtained through data rotations, which can be performed either clockwise or counter-clockwise, depending on the data distribution. Therefore, in order to establish a decision for the axis sense, we need to define some multivariate references for whom an ordering is known *a priori*. The references could be defined in a supervised or unsupervised way, for the entire image, so that the same references could be used for all the local pseudo-extrema estimations. In the supervised case the references could be defined according to the application goals, while in the unsupervised case, certain measures of the image data distribution may be used in order to define the references.

4.2.1. Global reference coordinates

Within this work, we chose an unsupervised approach for determining the global references by applying PCA on the entire image data $\mathcal{S}_{\mathcal{D}f} \subset \mathbb{R}^3$ (as a particular case of multivariate images). After this first step, we compute the Chebyshev bounds on each axis, in order to obtain a set of 3 pairs of coordinates, $((\widetilde{\mathfrak{R}^+_0}, \widetilde{\mathfrak{R}^-_0}), (\widetilde{\mathfrak{R}^+_1}, \widetilde{\mathfrak{R}^-_1}), (\widetilde{\mathfrak{R}^+_2}, \widetilde{\mathfrak{R}^-_2}))$, prioritized according to the variances on the respective directions and expressed in the $\widetilde{\mathcal{S}_{\mathcal{D}f}}$ coordinate system as

$$\begin{cases} \widetilde{\mathfrak{R}^+_0} = (\mu_{\widetilde{\xi_0}} + k\sigma_{\widetilde{\xi_0}}, 0, 0) \\ \widetilde{\mathfrak{R}^+_1} = (0, \mu_{\widetilde{\xi_1}} + k\sigma_{\widetilde{\xi_1}}, 0) \\ \widetilde{\mathfrak{R}^+_2} = (0, 0, \mu_{\widetilde{\xi_2}} + k\sigma_{\widetilde{\xi_2}}) \end{cases} \tag{11}$$

$$\begin{cases} \widetilde{\mathfrak{R}^-_0} = (\mu_{\widetilde{\xi_0}} - k\sigma_{\widetilde{\xi_0}}, 0, 0) \\ \widetilde{\mathfrak{R}^-_1} = (0, \mu_{\widetilde{\xi_1}} - k\sigma_{\widetilde{\xi_1}}, 0) \\ \widetilde{\mathfrak{R}^-_2} = (0, 0, \mu_{\widetilde{\xi_2}} - k\sigma_{\widetilde{\xi_2}}) \end{cases} \tag{12}$$

In the case of n-dimensional images, n pairs of reference coordinates have to be used. The discrimination between $\widetilde{\mathfrak{R}^+_i}$ and $\widetilde{\mathfrak{R}^-_i}$, in order to define which one could be chosen as the global supremum or infimum on the corresponding principal component, is based on the value of the third-order statistical moment, i.e. the skewness of the data on the corresponding direction. If the skewness on the direction given by $\overrightarrow{\widetilde{\mathfrak{R}^-_i}, \widetilde{\mathfrak{R}^+_i}}$ is positive, than $\widetilde{\mathfrak{R}^-_i}$ is chosen as the global infimum and $\widetilde{\mathfrak{R}^+_i}$ as the global supremum; otherwise, vice versa. The three pairs of coordinates, expressed in the initial coordinate system, $((\mathfrak{R}^+_0, \mathfrak{R}^-_0), (\mathfrak{R}^+_1, \mathfrak{R}^-_1), (\mathfrak{R}^+_2, \mathfrak{R}^-_2))$, are subsequently used as reference points within the local pseudo-morphological process.

4.2.2. Local pseudo-extrema

During the SE sweeping on the entire image, PCA is computed locally, on each of the multivariate data set, depending on the position of the SE ($\mathcal{D}_f \cap \mathcal{D}_g$). We chose to use only the first principal component generated by PCA and compute the Chebyshev interval on it, following the reasoning of using the PCA approach for data compression, in which the channels corresponding to the smallest variances are discarded, as they embed less energy than the ones corresponding to the largest variances [32]. Moreover, if we include more than one principal components within the processing, the number of the local pseudo-extrema would be larger than the number of axis, so an unicity problem for these extrema may appear. For instance, if we choose the first two principal components, four pseudo-extrema would result, two on each side of the mean, on each direction. This case is depicted in Fig. 7, where the pseudo-extrema choice in the case of the first (green dots) and the first two (red dots) principal components is presented, for two-dimensional data (blue dots). Consequently, the pseudo-extrema of the local data, after PCA ($\widetilde{\mathcal{S}_{\mathcal{D}_f \cap \mathcal{D}_g}}$), are computed as

$$\widetilde{\mathcal{E}_\alpha} = (\mu_{\widetilde{\xi}} + k\sigma_{\widetilde{\xi}}, 0, 0) \tag{13}$$

$$\widetilde{\mathcal{E}_\beta} = (\mu_{\widetilde{\xi}} - k\sigma_{\widetilde{\xi}}, 0, 0) \tag{14}$$

with $\widetilde{\xi}$ as the particular outcome of a random variable, modeling the first principal component of the local multivariate data. Going back to the original space, the pseudo-extrema $\mathcal{E}_\alpha$ and $\mathcal{E}_\beta$ would be

vectors within the initial multivariate space, thus resulting a full-vectorial processing.

4.2.3. Extrema labeling

As it was previously presented, the PCA gives only the directions in which the data has the largest variance, but it gives no sense for these directions, so we need to identify which of $\mathcal{E}_\alpha$ or $\mathcal{E}_\beta$ is the pseudo-supremum and which is the pseudo-infimum of the local multivariate data. The references are used at this level: a projection-like operation as a vectorial dot product is used, along with the *a priori* known references, in order to identify the desired ordering scheme. This process is expressed in the first branch of Eqs. (15) and (16), where $\overrightarrow{\mathfrak{R}_0^-\mathfrak{R}_0^+}$ represents the vector generated by the references $\mathfrak{R}_0^-$ and $\mathfrak{R}_0^+$, while $\overrightarrow{\mathfrak{R}_0^-\mathcal{E}_\alpha}$ and $\overrightarrow{\mathfrak{R}_0^-\mathcal{E}_\beta}$ are the vectors generated by the reference $\mathfrak{R}_0^-$ and the two local pseudo-extrema $\mathcal{E}_\alpha$ and $\mathcal{E}_\beta$. These vectors are depicted in Fig. 8. However, as the probability $p(\overrightarrow{\mathfrak{R}_0^-\mathfrak{R}_0^+} \perp \overrightarrow{\mathcal{E}^-\mathcal{E}^+})$ is not null and in the same manner, the probability $p(\overrightarrow{\mathfrak{R}_1^-\mathfrak{R}_1^+} \perp \overrightarrow{\mathcal{E}^-\mathcal{E}^+})$ is not null either, all the three reference pairs have to be taken into account within this process, so the other two branches in Eqs. (15) and (16) are appended in order to include these cases, too. These two branches of the equations are required in order to theoretically obtain the total order property between the estimated pseudo-extrema. For real images, there may appear cases where the pseudo-extrema generate vectors which are perpendicular on the vector generated by the first pair of references, therefore, we envisage the two alternative cases as a solution for this issue. Thus, the pseudo-erosion and the pseudo-dilation in the n-dimensional image case, for a particular $n=3$, are defined as

$$[\varepsilon_g(f)](x) = \bigwedge_{\substack{z\in D_g \\ x\in D_f}} f(x+z) \triangleq$$

$$= \begin{cases} \arg\min_i[\overrightarrow{\mathfrak{R}_0^-\mathfrak{R}_0^+}\cdot\overrightarrow{\mathfrak{R}_0^-i}], & i\in\{\mathcal{E}_\alpha,\mathcal{E}_\beta\} \\ \arg\min_i[\overrightarrow{\mathfrak{R}_1^-\mathfrak{R}_1^+}\cdot\overrightarrow{\mathfrak{R}_1^-i}], & i\in\{\mathcal{E}_\alpha,\mathcal{E}_\beta\} \text{ if } \overrightarrow{\mathfrak{R}_0^-\mathfrak{R}_0^+}\cdot\overrightarrow{\mathcal{E}_\alpha\mathcal{E}_\beta}=0 \\ \arg\min_i[\overrightarrow{\mathfrak{R}_2^-\mathfrak{R}_2^+}\cdot\overrightarrow{\mathfrak{R}_1^-i}], & i\in\{\mathcal{E}_\alpha,\mathcal{E}_\beta\} \text{ if } \overrightarrow{\mathfrak{R}_0^-\mathfrak{R}_0^+}\cdot\overrightarrow{\mathcal{E}_\alpha\mathcal{E}_\beta}=\overrightarrow{\mathfrak{R}_1^-\mathfrak{R}_1^+}\cdot\overrightarrow{\mathcal{E}_\alpha\mathcal{E}_\beta}=0 \end{cases} \tag{15}$$

$$[\delta_g(f)](x) = \bigvee_{\substack{z\in D_g \\ x\in D_f}} f(x-z) \triangleq$$

$$= \begin{cases} \arg\max_i[\overrightarrow{\mathfrak{R}_0^-\mathfrak{R}_0^+}\cdot\overrightarrow{\mathfrak{R}_0^-i}], & i\in\{\mathcal{E}_\alpha,\mathcal{E}_\beta\} \\ \arg\max_i[\overrightarrow{\mathfrak{R}_1^-\mathfrak{R}_1^+}\cdot\overrightarrow{\mathfrak{R}_1^-i}], & i\in\{\mathcal{E}_\alpha,\mathcal{E}_\beta\} \text{ if } \overrightarrow{\mathfrak{R}_0^-\mathfrak{R}_0^+}\cdot\overrightarrow{\mathcal{E}_\alpha\mathcal{E}_\beta}=0 \\ \arg\max_i[\overrightarrow{\mathfrak{R}_2^-\mathfrak{R}_2^+}\cdot\overrightarrow{\mathfrak{R}_1^-i}], & i\in\{\mathcal{E}_\alpha,\mathcal{E}_\beta\} \text{ if } \overrightarrow{\mathfrak{R}_0^-\mathfrak{R}_0^+}\cdot\overrightarrow{\mathcal{E}_\alpha\mathcal{E}_\beta}=\overrightarrow{\mathfrak{R}_1^-\mathfrak{R}_1^+}\cdot\overrightarrow{\mathcal{E}_\alpha\mathcal{E}_\beta}=0 \end{cases} \tag{16}$$

The complete processing chain for color images is presented in Fig. 9, with the two steps: the global processing in which the global references are computed and the local processing embedded inside the pseudo-morphological operators, in which the local pseudo-extrema are estimated.

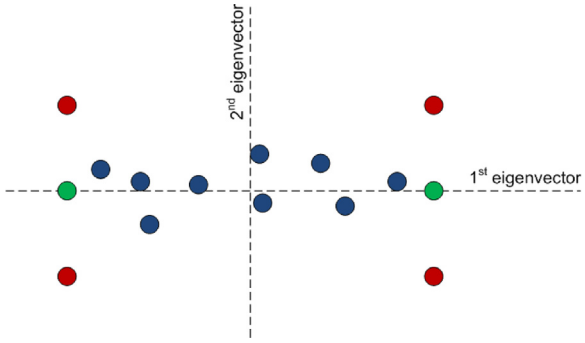

Fig. 7. Pseudo-extrema choice for the first (green dots) and the first two (red dots) principal components, for a two-dimensional data (blue dots) case. (For interpretation of the references to color in this figure caption, the reader is referred to the web version of this article.)

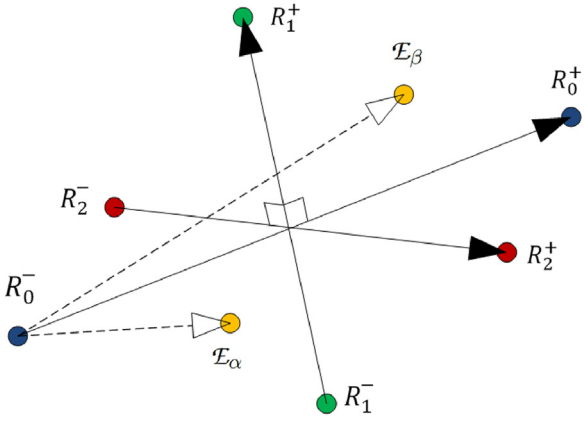

Fig. 8. The vectors generated by the references and by the local pseudo-extrema.

4.3. Qualitative results

There exists many extensions of the MM to multivariate images. However, there are few works in which a comparison between these extensions is performed, especially because there is no obvious criteria to compare them. In this section we present some results generated using our approach, from a qualitative point of view, analyzing the behavior of the basic operators according to the k parameter, which manages the pseudo-extrema estimation. We also compare the PPM with other existing morphological or pseudo-morphological approaches. After this qualitative analysis,

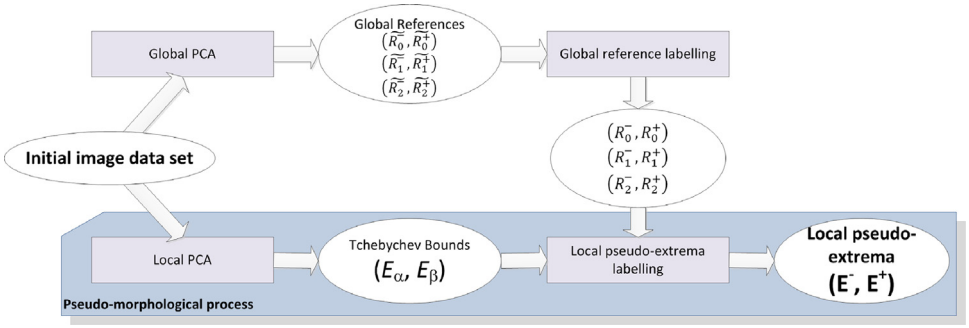

Fig. 9. The scheme to estimate the local pseudo-infimum and pseudo-supremum.

in the next section we present some quantitative results, obtained in texture analysis, segmentation and classification tasks.

In Figs. 11–14, we present several results generated using the pseudo-erosion and pseudo-dilation operations, with a square SE, applied on the original images from Fig. 10. All the operations are performed in the RGB color space, but any other color space may be used. We chose RGB for two reasons: first, the three coordinates are of the same nature, representing a quantity of a certain base color (for other spaces one component is the luminance and the others are chrominances, therefore, they are of different nature) and second, all of them are correlated and thus, adequate for the application of PCA. The first thing one could notice when comparing the four sets of results is that the pseudo-dilations applied on "Lena" and "Miro" enlighten the original images, while for the "Baboon" and "Candies", the image is darkened by the pseudo-dilation and enlightened by the pseudo-erosion. This happens because the discrimination between the references is performed according to the skewness of the global distributions, computed on the corresponding principal components. Nevertheless, in the color domain, this is the major problem when a decision has to be made for labeling two colors, one as the color corresponding to the dilation and the other one corresponding to the erosion i.e. to

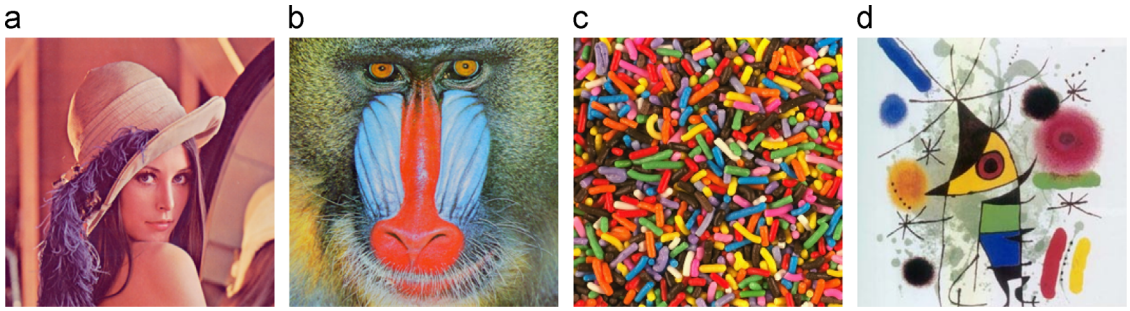

Fig. 10. Color test images. (a) Lena. (b) Baboon. (c) Candies. (d) Miro. (For interpretation of the references to color in this figure caption, the reader is referred to the web version of this article.)

Fig. 11. Pseudo-erosions (left half) and pseudo-dilations (right half), PPM, SE size is 5×5 (top row) and 11×11 (bottom row). (For interpretation of the references to color in this figure caption, the reader is referred to the web version of this article.)

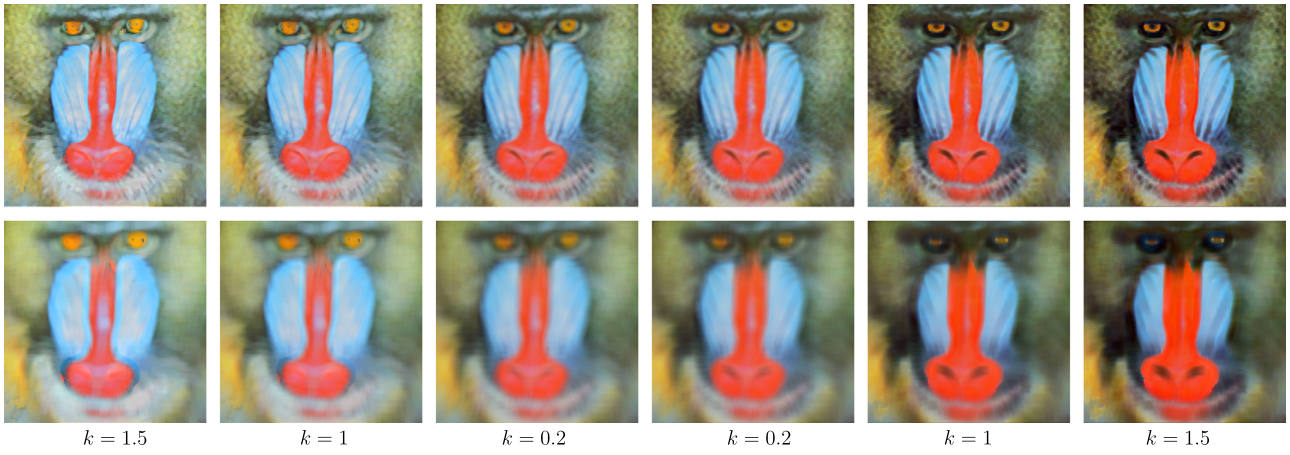

Fig. 12. Pseudo-erosions (left half) and pseudo-dilations (right half), PPM, SE size is 5×5 (top row) and 11×11 (bottom row). (For interpretation of the references to color in this figure caption, the reader is referred to the web version of this article.)

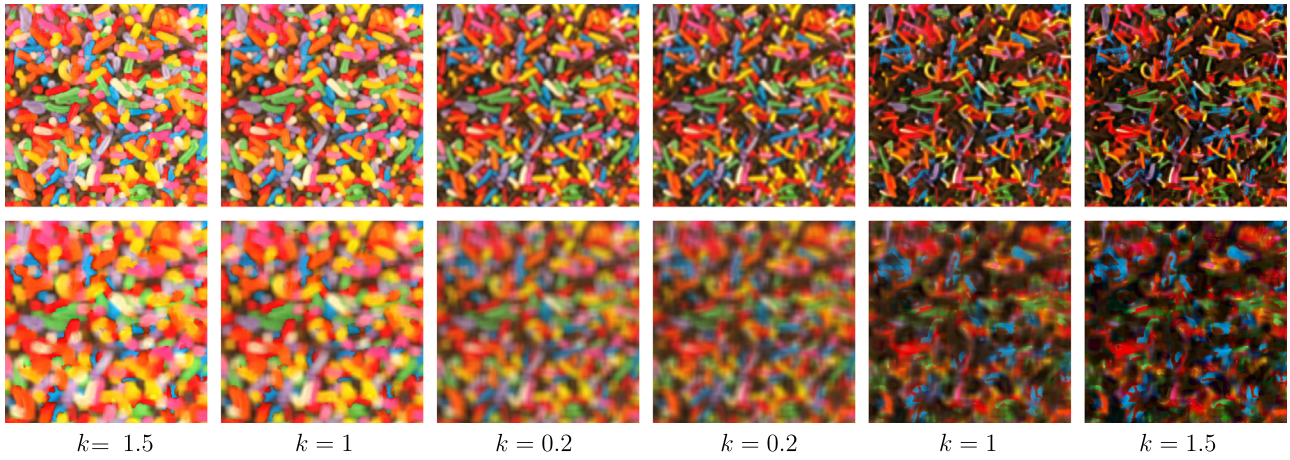

Fig. 13. Pseudo-erosions (left half) and pseudo-dilations (right half), PPM, SE size is 5×5 (top row) and 11×11 (bottom row). (For interpretation of the references to color in this figure caption, the reader is referred to the web version of this article.)

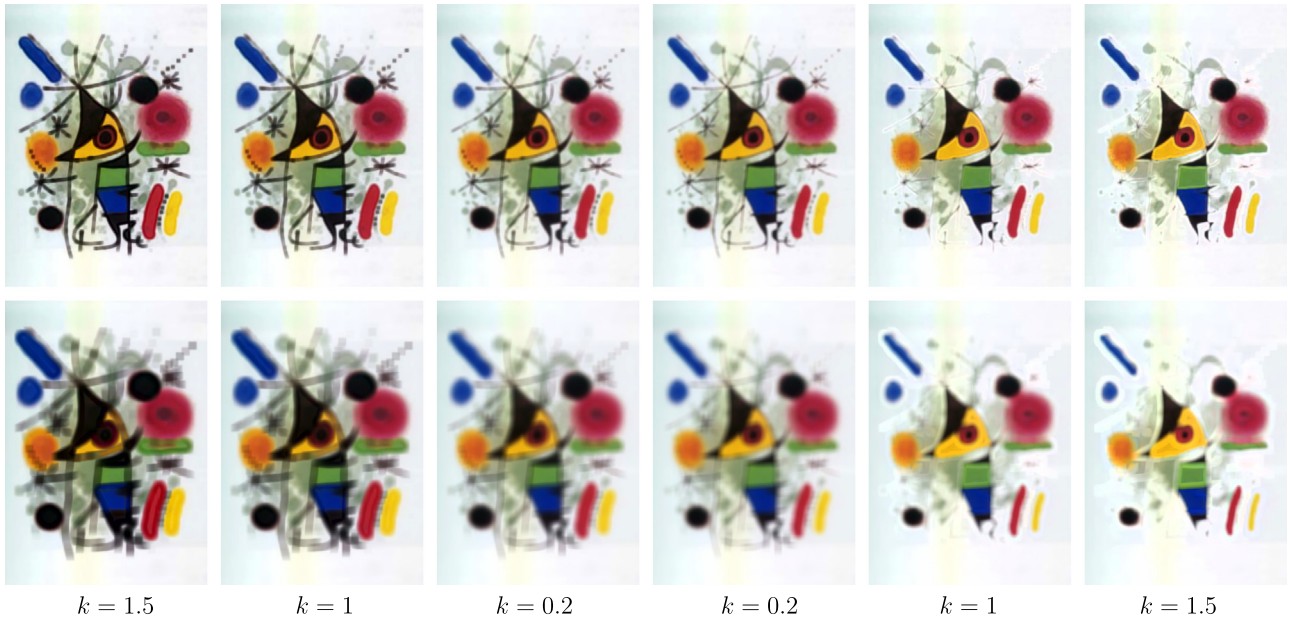

Fig. 14. Pseudo-erosions (left half) and pseudo-dilations (right half), PPM, SE size is 5×5 (top row) and 11×11 (bottom row). (For interpretation of the references to color in this figure caption, the reader is referred to the web version of this article.)

order the two colors. For instance, there is no obvious reason, from the human perception point of view, why the green color should be greater than the blue one, or vice versa, unless it is specified by the application. This is why we chose the skewness of the color distribution of the entire image as a discrimination criterion, independently of any higher level interpretation. By choosing the six references according to the global distribution for each image, we emphasize the fact that we could use other colors than the *classical* black and white as the supremum or infimum for each image. This fact could be noticed in the "Candies" pseudo-erosions, where red and orange hues are emphasized, while in "Baboon" pseudo-dilations, the red nose becomes more emphasized. As a remark regarding the reference points, we should say that for the results generated within this paper, we never reached a situation in which we applied the third or even the second cases of the relations (15) and (16) for the local processings. So, the second and the third pairs of the global reference points may not be used at all, leaving the first pair as the only global extrema of the processed images. As a final remark here, the six references and the order within each pair may also be chosen manually by the user, or according to the application specification.

Another observation to be made when analyzing the results is that the pseudo-dilations and pseudo-erosions visually behave as dual operations, since the objects filtered by one of them are emphasized by the other one. However, this emphasis is somehow attenuated by the filtering effect generated by the inclusion of the color distribution within each local processing. As an example, the pseudo-erosions of "Baboon" accentuate the light-colored hair, while the pseudo-dilation removes it. The pseudo-dilations and pseudo-erosions of "Miro" behave in a similar way with the corresponding grayscale morphological filters, the erosion removing the thin lines while the dilation enhances them.

The extension to the multivariate case inherited the k parameter from the grayscale case, and consequently it affects the results in the same manner: a small value for k generates images close to ones obtained through a linear smoothing filter for vectorial data, while the larger the k value, the more pronounced is the effect of the two pseudo-morphological operations, leading to a non-linear behavior. Therefore, it may be used as an adjustment within the design of linear and non-linear filters. However, for the multivariate case, large values for k may have some undesired effects: on the first hand, color saturation may occur, if the estimated local extrema are outside the

gamut/color space. These saturated colors may be computed either marginally, or by taking into consideration the direction of the local color distribution. In the latter case, there may appear problems when computing the intersection of this direction with the color space boundaries, which may be problematic for certain color spaces like CIELAB or CIELUV (see also [15]). On the other hand, the larger the k values, the farther the generated extrema would be from the colors within the given distribution, thus generating false colors which differ substantially from the colors in the initial distribution. We show in Fig. 15 that unlike the marginal approach [33], which may generate completely different colors than the ones from the initial distribution, color PPM generates colors which are visually related to the initial ones i.e. which are inside the tridimensional *cloud* of points determined by the color distribution. However this behavior strongly depends on the choice of the k parameter. For instance, one may notice within the "Baboon" pseudo-dilation, for $k=1.5$ and SE of size 11×11 that some dark blue shades appears around the eyes, which does not correspond with the initial image colors. Therefore, for this image $k=1$ would more adequate.

Due to the way color PPM computes the two local pseudo-extrema as complementary vectors, on one side and on the other of the vectorial mean, along the first principal component generated by PCA, the proposed pseudo-morphological operations are dual, implicitly exhibiting the property of duality (see [9] for a demonstration of the duality property). Furthermore, this approach may be successfully used in edge detection, through the morphological gradient operation, given by the difference between dilation and erosion, computed with the same SE. In our case of multivariate images, we may encounter certain situations in which one or more components of the pseudo-dilation may be smaller than the corresponding components of the pseudo-erosion. Therefore, we computed the gradient marginally, as the absolute value of the difference between pseudo-dilation and pseudo-erosion, on each color component. The top row of Fig. 16 depicts the resulted gradients, for our test images. It may be noticed that the gradient images are colored, due to the fact that the differences between pseudo-dilations and pseudo-erosions are computed marginally. The resulted colors are given by the orientation and *elongation* on the first principal component of the local distributions.

Another approach to generate the gradient is by computing the distance between the pseudo-dilations and pseudo-erosions for each pixel, which would generate a grayscale image consisting of values which are proportional to the standard deviations of the local distributions, along the first principal component. The bottom row of Fig. 16 depicts the resulted grayscale gradients, obtained after computing ΔE distances between pseudo-dilation and pseudo-erosion, pixel by pixel, in the CIELAB color space [34]. The conversion from RGB to CIELAB was performed using illuminant $D65$.

In Fig. 17 we compare, from a qualitative point of view, our approach with two color MM approaches, which use the lexicographical ordering in HSV color space, setting the color channels priorities to (V,S,H) for one case and (H,V,S) for the other [35,36].

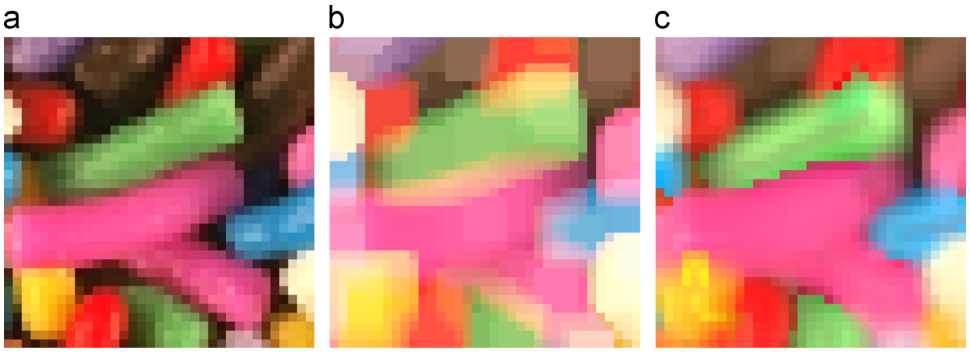

Fig. 15. False colors introduced by our approach and by the classical marginal MM – crop from the "Candies" image. (a) Original, (b) marginal, and (c) PPM. (For interpretation of the references to color in this figure caption, the reader is referred to the web version of this article.)

Fig. 16. Color and grayscale morphological gradients for 3×3 SE, computed marginally (top row) and using CIELAB ΔE distance (bottom row). (For interpretation of the references to color in this figure caption, the reader is referred to the web version of this article.)

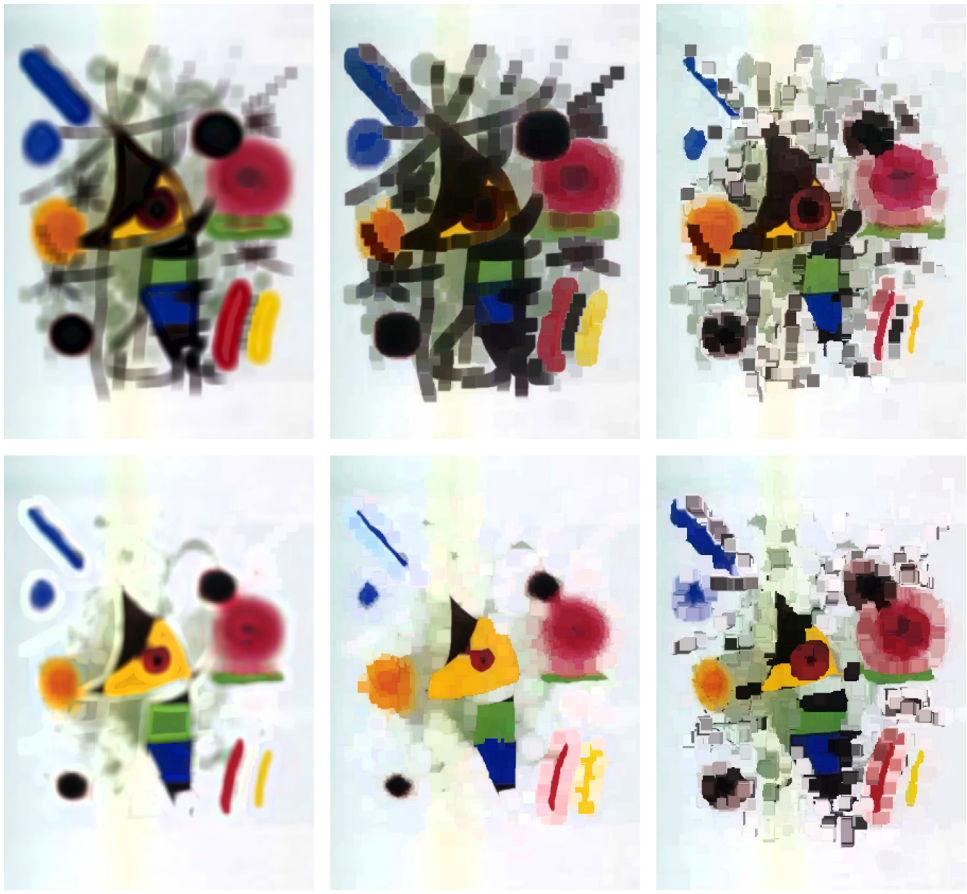

Fig. 17. Erosions/pseudo-erosion (top row) and dilations/pseudo-dilation (bottom row) for PPM ($k=1.5$, 11×11 SE) and lexicographical ordering (VSH and HVS priorities).

One may notice that the results obtained with the PPM approach are visually similar to the ones obtained using the (V,S,H) priority. Moreover, PPM preserves the shapes better, generating more consistent results, which do not depend on the channel priorities. The results for the (H,V,S) priority are more sensitive to hue differences.

4.4. Quantitative results

In this section we quantitatively assess the performance of our color PPM approach and compare it with other morphological and pseudo-morphological methods. As explained in [37], it is difficult to perform a quantitative comparison between morphological approaches only through the results given by their basic operations, because there is no obvious criteria to apply in order to generate which approach is better. Therefore, for a quantitative assessment, the impact of the morphological operations in image analysis tasks has to be estimated through derived operations which generate quantifiable results. Thus, in what follows, we compare our color approach with other methods using three criteria: color fractal dimension estimation, color textured image segmentation and color texture classification.

4.4.1. Accuracy on fractal dimension estimation

Analogous to the grayscale case, we chose the FD of color fractal images as a measure to validate the color PPM. Color fractal images were introduced in [38], where they were generated through an extension of the *random midpoint displacement* algorithm described in [30]. The H parameter ($H\in[0,1]$) is also used in this case, adjusting the complexity of the generated texture. The FD for color images varies between 2 and 5: a color FD close to 5 is obtained for highly complex textures, obtained with $H\to0$, while a FD with a value of 2 is generated with $H\to1$. The upper dimension is 5 because the color images are 5-dimensional fractal objects, comprised within the space generated by the three color components (R, G and B in our case) and the two spatial coordinates within the image (x and y). In Fig. 18 several FDs estimations are depicted as a function of H. The FDs are estimated using four approaches: *covering blanket* using PPM, the lexicographical MM in HSV color space, with (V,S,H) priority among channels and $\alpha-$trimmed pseudo-morphology [20] and the color box-counting algorithm [38]. The $\alpha-$trimmed algorithm was applied in the RGB color space, with α automatically computed as described in the cited paper. It may be noticed that our approach has the highest dynamic range, as a function of the H parameter. This means that it may be successfully used as a texture feature for color texture complexity ranking and discrimination. However, the maximum and the minimum values are not closed to 5 and 2, as expected. The reason is that the color fractal images are not continuous objects as in theory, so due to the quantization and sampling errors, the high complexity is lost and consequently, the FD is underestimated. For low complexity textures the FD is overestimated due to a limitation intrinsic to the *covering blanket* estimation algorithm.

4.4.2. Textured image segmentation

Next, we present our results regarding the quantitative evaluation of the impact of our proposed approach in the framework of color textured image segmentation. We compare our approach with the $\alpha-$trimmed pseudo-morphology, computed in RGB color

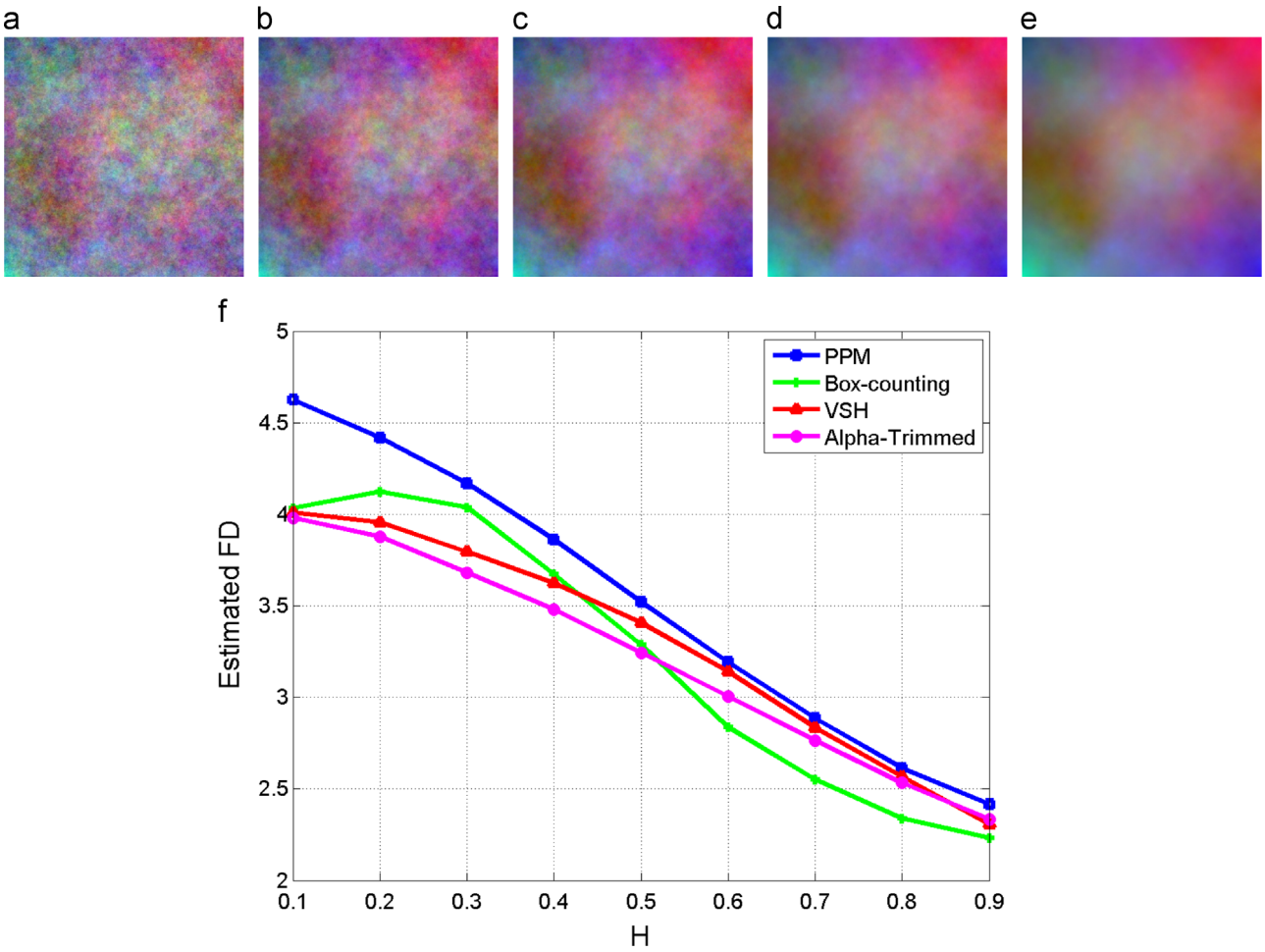

Fig. 18. FD estimation comparison using four different approaches, as a function of the Hurst parameter H, for color textures of varying complexity (top row). (a) $H=0.1$, (b) $H=0.3$, (c) $H=0.5$, (d) $H=0.7$, (e) $H=0.9$, and (f) comparison. (For interpretation of the references to color in this figure caption, the reader is referred to the web version of this article.)

space and with the lexicographical morphological approach, using the HSV color space with (V,S,H) component priority. We performed image segmentation based on local texture features. As texture features, we used the vector of volumes computed between pseudo-dilation and pseudo-erosion, for varying sizes of the SE. We used this feature due to the fact that it reflects the texture complexity, since in the log–log space, it allows the estimation of the FD of the given texture. However, as for real textures the fractal hypothesis does not stand, we chose to use the entire vector, which comprises more information than the FD by itself. We used textured images from the Berkeley database [39], in which there is a salient object and the background. Our first attempt is to discriminate between *simple* (out of focus regions) and *complex* (in focus object). Thus, we computed the vectors for local regions within the images, using sliding window, followed by a k-means classification in two classes. We computed the segmentations using PPM, α−trimmed and (V,S,H) lexicographical ordering. We also generated a ground-truth segmentation, performed by a human, which is used as a reference for a quantitative comparison among the three approaches. The results are depicted in Fig. 19.

As a quantitative comparison, we computed the percentage of correctly classified pixels as a segmentation evaluation criterion, as in [40]. The results are presented in Table 2. One may notice that in the most of the cases, PPM leads to a better segmentation, proving the increased ability to capture the complexity of textures and variation along scales. Segmentation could be further improved, by considering the window size used for local feature computation.

4.4.3. Color texture classification

In order to demonstrate the usefulness of our pseudo-morphological approach for texture description and classification we chose the normalized morphological covariance [22], recently extended to color images [20]. By definition, the morphological covariance is the volume of an eroded image, using a pair of points $P_{2,\vec{v}}$ separated by a vector $\vec{v}$, as SE: $[K(f)][\vec{v}]=V_{\varepsilon_{P_{2,\vec{v}}}}$. However, since in PPM we need a distribution of a set in order to estimate the two pseudo-extrema, we embrace the approach proposed by [20], in which a pair of SEs separated by a vector $\vec{v}$ is used instead of just two points. In addition, K is normalized according to the volume of the initial image. For the volume computation we propose to use the volume between the initial image and the pseudo-eroded image, in order to better capture the differences between the initial and the resulted colors, after pseudo-erosion. We compute the normalized covariance using four orientations for $\vec{v}$ (0°, 45°, 90°, 135°) and 25 iterations on each orientation, varying the module of $\vec{v}$ with a step of two pixels, thus resulting a K vector of size 100. We performed two experiments:

(i) First, we perform the classification on the Outex13 color texture database, which consists of 68 textures, each divided into 20 non-overlapping sub-images of 128×128 pixels, thus resulting

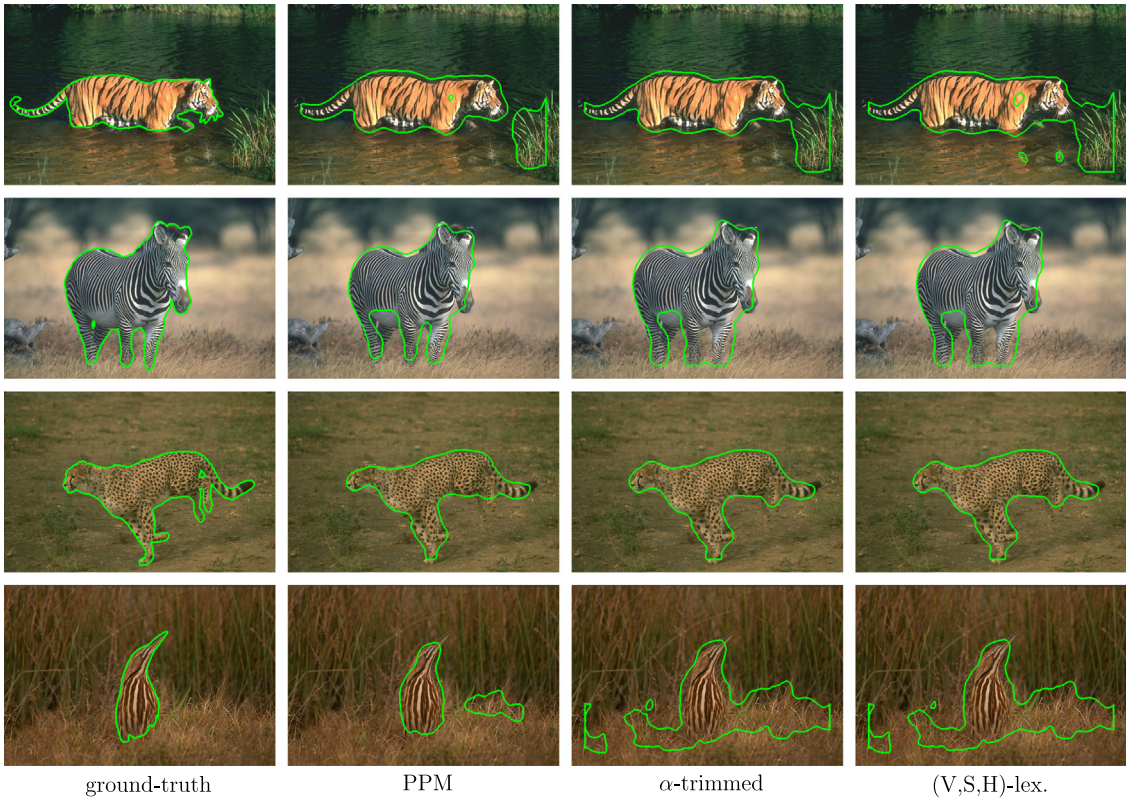

Fig. 19. Segmentations based on local texture features obtained using PPM, $\alpha-$trimmed pseudo-morphology and (V,S,H) lexicographical morphology for Berkeley 108073 (first row), 130066 (second row), 134008 (third row), and 43033 (fourth row) images.

Table 2
Percentage of correctly classified pixels, for the four images in Fig. 19.

Image	PPM (%)	$\alpha-$trimmed (%)	(V,S,H) lex. (%)
Berkeley 108073	92.37	91.41	90.57
Berkeley 130066	96.06	95.37	95.40
Berkeley 134008	96.53	96.86	96.90
Berkeley 43033	96.35	86.01	86.19

1360 images to be classified [41]. We computed the normalized covariance for each of the 1360 sub-images, using PPM, $\alpha-$trimmed and (V,S,H) lexicographical morphology. We use half of the resulted vectors as training samples and half of them as test samples, within the out-of-the-box discriminant analysis available in MATLAB, obtaining approximately the same good classification rates for all the three used approaches (76.76% for PPM, 76.32% for $\alpha-$trimmed and 76.47% for (V,S,H) lexicographical morphology). In conclusion, this experiment shows that our approach generates a comparable result with the ones given by the other two approaches.

(ii) In order to focus on the extracted morphological features rather than on the classification process itself, we embraced the protocol proposed by [42]. In addition, taking into consideration that in the Outex13 database there are many visually similar images which are considered as different textures (e.g. the sandpaper or the barley-rice textures) we performed another experiment in which we chose nine classes of color textures from the Outex database (barleyrice, canvas, carpet, chips, fur, granite, plastic, seeds and wood), with 8 images from each class. These images were split into 20 sub-images of size 128×128, thus resulting 1440 samples. We computed the morphological covariance for each of these samples and we used half of the resulted vectors as training set and half of them as test set. Using this set of textured images and the generalized co-occurrence matrix along with the classification protocol described in [42] we obtained a good classification rate of 88.27%, which we further use as reference. The good classification rate obtained using PPM is 81.38%, while the result obtained using $\alpha-$trimmed pseudo-morphology is 68.5%. However, given that our morphological covariance is based only on color differences, being invariant to the actual colors within the textures, we added the first and the second probabilistic moments of each color channel within the feature vector. The obtained results for good classification rates are 92.36% for PPM and 78.47% for $\alpha-$trimmed. In conclusion, the morphological covariance obtained using our PPM leads to a worse result than the one obtained using the generalized co-occurrence matrix, but by adding the color information, we are able to obtain a higher good classification rate. In this particular context, our approach shows a better contribution to textural feature extraction than the $\alpha-$trimmed pseudo-morphology.

5. Discussion

5.1. Marginal, vectorial, false colors

First of all, our proposed approach is a full-vectorial approach. This was one of the design goals, in order to avoid the drawbacks of the marginal approaches. The expressions (15) and (16) are similar to a classical lexicographic ordering: indeed, our approach may be interpreted as a lexicographical ordering on the principal components. However, in our case, the different subparts exist in order to completely identify which local pseudo-extremum should be assigned to the infimum or supremum. In addition, even if the local pseudo-extrema, expressed in PCA basis, include two null values within their components, due to the fact that they are chosen on the first principal component, when they are expressed

in the initial coordinates, these components become non-null and thus, the approach is full-vectorial. As the process defines the pseudo-extrema through a probabilistic step, there is a certain probability that these extrema do not belong to the initial data set, so false colors are introduced. This issue appeared at the beginning of the color mathematical morphology with the marginal approaches that create color artifacts, thus degrading the morphological results. Within the PPM, the estimated pseudo-extrema, even if they are false colors, they are inside the distribution hull and pertinently close to the original colors, therefore, they cannot be perceived as a color degradation, for appropriate k parameters. The fractal criterion, that computes the accuracy of this construction in a multiscale morphological feature extraction shows that there is no problem with these false colors from a metrological point of view. Furthermore, the false color generation may be avoided by adding a new constraint for Eqs. (15) and (16), in order to choose a color from the initial distribution (e.g. the closest color to the pseudo-extrema). However, such a construction would lead to other problems, such as ensuring the unicity of the chosen extrema.

5.2. The labeling of global extrema

In order to completely identify which of the pseudo-extrema should be defined as the local supremum or infimum, a set of global references is required. Different pre-processing steps may solve this problem: as many of the existing approaches induce orders around the luminance axis, one solution for this labeling would be to classify the references according to their distances to black and white. Also, when the application objectives are well defined, with reproducible content and well-managed illumination conditions, the labeling process could be manually driven. This manual process would allow the user to specify what distribution part corresponds to the objects of interest or to the background. Thus, the references could be ordered in an unsupervised or supervised mode. There are several possible unsupervised ways of labeling the two points, but in this work, for illustration, we used the skewness of the distribution. If the distribution is asymmetrical, this measure allows to associate a global image supremum with the representative side of the distribution. Thus, it generates a pseudo-morphological approach which is totally driven by the statistical properties of the image data. One of the disadvantages of our probabilistic approach lies in the fact that the results are not linked to the application objective or to the image understanding from the user's point of view.

5.3. The approach complexity

The classical PCA algorithm has a complexity of $O(n^3+n^2\times M)$ for M n-dimensional points, taking into account that we do not reduce the feature space dimension. However, this is not a real problem, due to the existence of Fast PCA algorithms [43]. In addition, like all the morphological operations, this process is also highly parallelizable. Therefore, the complexity of our approach is given by the local computation of PCA, which depends on the SE size.

5.4. The total order property

As we have previously explained, in this pseudo-morphological construction, we do not order all the data inside the initial set. We define a pseudo-supremum and a pseudo-infimum and due to the construction, we ensure that these pseudo-extrema are unique. By using the Eqs. (15) and (16) we ensure that a total order relation exists among the estimated pseudo-extrema.

5.5. The choice of the color space

There exists a plethora of combinations of ordering approaches and color spaces used for color MM. Within this work, we chose to work in the RGB color space for various reasons: due to the correlations which exist among the color channels (which makes this color space adequate for the application of PCA) and due to the color construction of our extrema, particularly when we have to deal with special cases like large k values, in which a saturation has to be obtained.

As we use a PCA before each step of pseudo-extremum identification and labeling, we dynamically choose the right color representation through a linear transformation of the initial RGB color space. So all the existing color spaces which are derived through linear transformations from the RGB space are equivalent according to this approach. In addition, as we do not integrate any additional information about the illumination conditions for the processed images, the transformation from RGB to color spaces like XYZ would be performed with errors based on the real used white reference. Nevertheless, for specific applications, where this problem of illumination conditions knowledge could be solved, these kind of color spaces allow the usage of the perceptual distance, which solves the question of the color norm or distance validity from the RGB or equivalent color spaces.

6. Conclusion

We propose a probabilistic pseudo-morphology based on the Chebyshev's inequality, which allows to estimate a pseudo-supremum and a pseudo-infimum of a given set. The approach is based on the fact that for the basic morphological operations, only a supremum and an infimum of a data set are required, so instead of ordering the set we estimate the two extrema based on the statistical properties of the set. Our approach embeds both a linear and a non-linear behavior, given by the parameter k, which controls the error in extrema estimation, with respect to the actual maximum and minimum values of a set.

In order to validate our approach for grayscale images, we computed the quadratic error between the pseudo-dilation and pseudo-erosion based on the probabilistic extrema estimation, and the results of the same operations implemented using the classical MM (GLMM). In addition, for validation, we used the *covering blanket* approach for estimating the fractal dimension of fractal images. By comparison with the GLMM, our approach generates a better dynamic range and a behavior closer to the theoretical one, for synthetic fractal images.

We proposed a generic extension of the approach to a multi-dimensional space. In particular, for the extension to color domain, which has a particular interpretation for the human perception, our approach introduces false colors and some of the resulting colors may be outside the color space, according to the k parameter choice. However, we show how the estimation of the extrema is pertinent with respect to the color content, therefore the false colors generation is not really a drawback. The main interest of our probabilistic pseudo-morphology is in texture analysis tasks. Therefore, we used the proposed approach in color texture complexity estimation, textured image segmentation and texture classification, and showed that PPM offers comparable or even better results in particular cases.

Conflict of interest

None declared.

References

[1] G. Matheron, Random Sets and Integral Geometry, John Wiley and Sons, Inc., 1975.
[2] J. Serra, Image Analysis and Mathematical Morphology, vol. I, Academic Press, 1982.
[3] J. Goutsias, H.J.A.M. Heijmans, Fundamenta morphologicae mathematicae, Fundamenta Informaticae – Special Issue on Mathematical Morphology 41 (2000) 1–31.
[4] S. Sternberg, Grayscale morphology, Computer Vision, Graphics, and Image Processing 35 (1986) 333–355.
[5] R. Haralick, S. Sternberg, X. Zhuang, Image analysis using mathematical morphology, IEEE Transactions on Pattern Analysis and Machine Intelligence 9 (1987) 532–550.
[6] P. Maragos, R. Schafer, Morphological filters–part I: their set-theoretic analysis and relations to linear shift-invariant filters, IEEE Transactions on Acoustics, Speech and Signal Processing 35 (1987) 1153–1169.
[7] F. Meyer, S. Beucher, The morphological approach of segmentation: the watershed transformation, in: E. Dougherty (Ed.), Mathematical Morphology in Image Processing, Marcel Dekker, New York, 1992.
[8] V. Barnett, The ordering of multivariate data, Journal of the Royal Statistical Society 139 (1976) 318–355.
[9] M. Ivanovici, A. Caliman, N. Richard, C. Fernandez-Maloigne, Towards a multivariate probabilistic morphology for colour images, in: Proceedings of the 6th European Conference on Colour in Graphics, Imaging and Vision, Amsterdam, The Netherlands, 2012, pp. 189–193.
[10] A. Ledoux, N. Richard, A.S. Capelle-Laize, Limits and comparisons of orderings using colour distances, Traitement du Signal 29 (2012) 65–82.
[11] J.J. van de Gronde, J.B.T.M. Roerdink, Group-invariant frames for colour morphology, in: C.L. Hendriks, G. Borgefors, R. Strand (Eds.), Mathematical Morphology and Its Applications to Signal and Image Processing, Lecture Notes in Computer Science, vol. 7883, Springer, Berlin, Heidelberg, 2013, pp. 267–278.
[12] E. Aptoula, S. Lefèvre, A comparative study on multivariate mathematical morphology, Pattern Recognition 40 (2007) 2914–2929.
[13] S. Velasco-Forero, J. Angulo, Random projection depth for multivariate mathematical morphology, IEEE Journal of Selected Topics in Signal Processing 6 (2012) 753–763.
[14] O. Lezoray, C. Charrier, A. Elmoataz, Learning complete lattices for manifold mathematical morphology, in: M. Wilkinson, J. Roerdink (Eds.), Proceedings of the 9th International Symposium on Mathematical Morphology, ISMM '09, University of Groningen, The Netherlands, 2009, pp. 1–4.
[15] B. Burgeth, A. Kleefeld, Morphology for color images via Loewner order for matrix fields, in: C.L. Hendriks, G. Borgefors, R. Strand (Eds.), Mathematical Morphology and Its Applications to Signal and Image Processing, Lecture Notes in Computer Science, vol. 7883, Springer, Berlin, Heidelberg, 2013, pp. 243–254.
[16] S. Velasco-Forero, J. Angulo, Morphological processing of hyperspectral images using kriging-based supervised ordering, in: IEEE International Conference on Image Processing, Hong Kong, 2010, pp. 1409–1412.
[17] S. Velasco-Forero, J. Angulo, Supervised ordering in $\mathbb{R}^p$: application to morphological processing of hyperspectral images, IEEE Transactions on Image Processing 20 (2011) 3301–3308.
[18] A. Hanbury, J. Serra, Morphological operators on the unit circle, IEEE Transactions on Image Processing 10 (2001) 1842–1850.
[19] J. Angulo, Pseudo-morphological image diffusion using the counter-harmonic paradigm, in: J. Blanc-Talon, D. Bone, W. Philips, D. Popescu, P. Scheunders (Eds.), Advanced Concepts for Intelligent Vision Systems, Lecture Notes in Computer Science, vol. 6474, Springer, Berlin, Heidelberg, 2010, pp. 426–437.
[20] E. Aptoula, S. Lefèvre, α–trimmed lexicographical extrema for pseudo-morphological image analysis, Journal of Visual Communication and Image Representation 19 (2008) 165–174.
[21] A. Plaza, P. Martinez, R. Perez, J. Plaza, A new approach to mixed pixel classification of hyperspectral imagery based on extended morphological profiles, Pattern Recognition 37 (2004) 1097–1116.
[22] P. Soille, Morphological Image Analysis: Principles and Applications, Springer-Verlag, 2002.
[23] H.J.A.M. Heijmans, C. Ronse, The algebraic basis of mathematical morphology. 1 – dilations and erosions, Computer Vision, Graphics, and Image Processing 50 (1990) 245–295.
[24] P. Chebyshev, Des valeurs moyennes, Journal de Mathematiques Pures et Appliquees 2 (1867) 177–184.
[25] A. Papoulis, Probability, Random Variables, and Stochastic Processes, 3rd edition, McGraw-Hill, 1991.
[26] S. Peleg, J. Naor, R. Hartley, D. Avnir, Multiple resolution texture analysis and classification, IEEE Transactions on Pattern Analysis and Machine Intelligence PMI 6 (1984) 518–523.
[27] P. Maragos, F. Sun, Measuring the fractal dimension of signals: morphological covers and iterative optimization, IEEE Transactions on Signal Processing 41 (1993) 108–121.
[28] A. Ledoux, N. Richard, S. Capelle-Laizé, C. Fernandez-Maloigne, Validation et limitation de métriques couleur pour l'ordonnancement, in: GRETSI – 23 Colloque sur le traitement du signal et des images, France, 2011.
[29] T. Peli, Multiscale fractal theory and object characterization, Journal of Optical Society of America 7 (1990) 1101–1112.
[30] H. Peitgen, D. Saupe, The Sciences of Fractal Images, Springer Verlag, 1988.
[31] A. Pentland, Fractal-based description of natural scenes, IEEE Transactions on Pattern Analysis and Machine Intelligence 6 (1984) 661–674.
[32] A.K. Jain, Fundamentals of Digital Image Processing, Prentice-Hall, Englewood Cliffs, NJ, 1989.
[33] C. Gu, Multivalued morphology and its application in moving object segmentation and tracking, in: P. Maragos, R. Schafer, M. Butt (Eds.), Mathematical Morphology and Its Applications to Image and Signal Processing, Computational Imaging and Vision, vol. 5, Springer, US, 1996, pp. 345–352.
[34] R. Seve, Practical formula for the computation of CIE 1976 hue difference, Color Research and Application 21 (1996) 314.
[35] J. Angulo, Morphological colour operators in totally ordered lattices based on distances: application to image filtering, enhancement and analysis, Computer Vision and Image Understanding 107 (2007) 56–73.
[36] G. Louverdis, M. Vardavoulia, I. Andreadis, P. Tsalides, A new approach to morphological color image processing, Pattern Recognition 35 (2002) 1733–1741.
[37] A. Ledoux, N. Richard, A.S. Capelle-Laize, The fractal estimator: a validation criterion for the colour mathematical morphology, in: Conference on Colour in Graphics, Imaging, and Vision 2012, 2012, pp. 206–210.
[38] M. Ivanovici, N. Richard, Fractal dimension of colour fractal images, IEEE Transactions on Image Processing 20 (2011) 227–235.
[39] D. Martin, C. Fowlkes, D. Tal, J. Malik, A database of human segmented natural images and its application to evaluating segmentation algorithms and measuring ecological statistics, in: Proceedings of 8th International Conference on Computer Vision, vol. 2, 2001, pp. 416–423.
[40] A. Carleer, O. Debeir, E. Wolff, Assessment of very high spatial resolution satellite image segmentations, Phogotrammetric Engineering and Remote Sensing 71 (2005) 1285–1294.
[41] T. Ojala, T. Mäenpää, M. Pietikäinen, J. Viertola, J. Kyllönen, S. Huovinen, Outex – new framework for empirical evaluation of texture analysis algorithms, in: Proceedings of the 16th International Conference on Pattern Recognition, vol. 1, ICPR02, IEEE Computer Society, Washington, DC, USA, 2002.
[42] V. Arvis, C. Debain, M. Berducat, A. Benassi, Generalization of the cooccurrence matrix for colour images: application to colour texture classification, Image Analysis and Stereology 23 (2011).
[43] A. Sharma, K.K. Paliwal, Fast principal component analysis using fixed-point algorithm, Pattern Recognition Letters 28 (2007) 1151–1155.

Alexandru Căliman received the B.Sc. and M.Sc. degrees from the Transilvania University, Braşov, România, in 2009 and 2011 respectively. He is currently a Ph.D. student at the same university. His research interests include color image processing and analysis through mathematical morphology and texture characterization.

Mihai Ivanovici received the B.Sc. degree from the Transilvania University, Braşov, România, then his M.Sc. and Ph.D. degrees from the Politehnica University, Bucureşti, România, in 2001, 2002 and 2006 respectively. His research interests include color image processing and analysis, with application in medicine and computer vision. He is assistant professor and head of MIV^2 Laboratory at Department of Electronics and Computers, Transilvania University, Braşov, România.

Noël Richard received the M.Sc and Ph.D. degrees from the University of Poitiers in 1988 and 1993 respectively. Since 1992, he is researcher at XLIM-SIC UMR CNRS 7552 laboratory. His research interests include non-linear image processing, mathematical morphology, fractal geometry and multi-scale texture features for color and multivariate images. Since 2000, his work focuses on human perception of colors and textures and the link between images and semantics through ontology and accuracy integration in the image processing scheme.